JOURNAL OF GEOPHYSICAL RESEARCH, VOL. 100, NO. D5, PAGES 8977–8991, MAY 20, 1995

# Comparison of measured and calculated aerosol properties relevant to the direct radiative forcing of tropospheric sulfate aerosol on climate

P. K. Quinn[1], S. F. Marshall[2], T. S. Bates[1,2], D. S. Covert[2], and V. N. Kapustin[1]

**Abstract.** The accuracy of the estimated radiative forcing of tropospheric sulfate aerosol depends on the quality and spatial coverage of the aerosol chemical, physical, and optical data that serve as input to global climate models. To augment the available data and to provide a comparison of measured and calculated optical properties, surface measurements were made of the aerosol light scattering and backscattering coefficients, the number size distribution from 0.02 to 9.6 μm, and chemical mass size distributions during two Pacific Ocean field experiments. All measurements were made on an aerosol sample stream dried to 30% relative humidity and are reported as such. The first experiment took place during the Pacific Sulfur/Stratus Investigation at Cheeka Peak, Washington, in April and May of 1991 (PSI 91). The second occurred as part of the Marine Aerosol and Gas Exchange cruise in February and March of 1992 (MAGE 92) which was conducted from 33°N to 12°S along 140°W. The mass size distributions of nonseasalt sulfate and sodium varied widely both spatially and temporally. The shape of the number size distribution remained fairly constant throughout both experiments with an accumulation mode geometric number mean diameter of 0.19 ± 0.03 μm and a geometric mean standard deviation of 1.4 ± 0.06. Measured light scattering and backscattering ranged from 3.7 to 19 × $10^{-6}$ $m^{-1}$ and 0.64 to 2.8 × $10^{-6}$ $m^{-1}$, respectively, resulting in an average backscattered fraction of 0.15 with a standard deviation of ±0.009. The light scattering and backscattering coefficients were calculated from a Mie model applied to the measured number size distributions. The mean of the calculated scattering values was 3% higher than the mean of the measured values with a 14% variance about the mean. This variance was within the uncertainty of the calculations indicating that the scattering characteristics of the aerosol were parameterized adequately by the model. The calculated backscattering values were about 40% lower than the measured values, however. The calculated light scattering apportioned to nonseasalt sulfate aerosol was 39 ± 17% of the total calculated scatter. The scattering to mass ratio for sulfate aerosol averaged 5.0 $m^2$ $g^{-1}$ with a standard deviation of ±1.6 $m^2$ $g^{-1}$ and varied with variability in the number size distribution. Further measurements are needed that will allow for the formation of a global-scale database to reveal the extent of the variability in the aerosol chemical, physical, and optical properties relevant to climate forcing.

## 1. Introduction

Tropospheric nonseasalt sulfate (nss $SO_4^=$) aerosols can affect climate directly by scattering incoming shortwave solar radiation and reflecting a portion of it back to space [*Charlson et al.*, 1991]. The reflected flux due to nss $SO_4^=$ aerosol, $\Delta F_R$, is proportional to the hemispheric backscattered fraction of incoming radiation, $b$, and the scattering to mass ratio of the sulfate ion, $\alpha_{sp,SO4,ion}$,

$$\Delta F_R \propto b\alpha_{sp,SO4,ion} \tag{1}$$

Traditionally, $\alpha_{sp,SO4,ion}$ has been defined as

$$\alpha_{sp,SO4,ion} = \frac{\sigma_{sp}}{m_{SO4}} \tag{2}$$

[*Waggoner et al.*, 1976] where $m_{SO4}$ includes only the mass of the $SO_4^=$ ion and no associated water or cationic species. The value $\sigma_{sp}$ is the measured total light scattering coefficient and is assumed to be an additive result of all scattering species $i$ present such that

$$\sigma_{sp} = \sum_i \sigma_{sp,i} \tag{3}$$

Alternatively, $\alpha_{sp,SO4,ion}$, can be defined as the light scattering due to sulfate aerosol per unit mass of sulfate ion (see Section 2.2). For the scattering to be additive, it is assumed that the aerosol is externally mixed, that is, the different particle species reside in different particle populations [*White*, 1986]. This assumption simplifies calculations but may not accurately describe the ambient aerosol. Scattering due to species within an internally mixed aerosol may not be additive in a linear fashion. *Sloane* [1984] has determined that the nonadditivity of the scattering contributed by sulfates may affect calculated values of scattering to mass ratios by 10%.

[1]Pacific Marine Environmental Laboratory, NOAA, Seattle, Washington.
[2]Department of Atmospheric Sciences, University of Washington, Seattle.



Paper number 95JD00387.
0148-0227/95/95JD-00387$05.00

Recently, estimates from two independent model calculations of the magnitude of the climate forcing due to sulfate aerosols have been reported [*Charlson et al.*, 1991; *Kiehl and Briegleb*, 1993]. The results from both models indicate that in many regions of the northern hemisphere, the cooling due to anthropogenic sulfate aerosol is comparable to the warming resulting from increased concentrations of greenhouse gases. While there is good agreement in the spatial variability predicted by the two models, the calculated magnitude of the forcing differs by a factor of 2. *Kiehl and Briegleb* [1993] explain that the disagreement is due, in part, to the use of different values of $\alpha_{sp,SO4,ion}$ and $b$.

*Charlson et al.* [1991] derive a value of 5 $m^2 g^{-1}$ for $\alpha_{sp,SO4,ion}$ based on measurements of sulfate haze over northern Europe [*Waggoner et al.*, 1976] and (2). This value is based on measurements of dried air and must be adjusted to account for ambient relative humidity. Observations from urban regions indicate that $\alpha_{sp,SO4,ion}$ increases by a factor of 1.7 as relative humidity (RH) increases from 50 to 80% [*Charlson et al.*, 1984]. Based on a mean RH for the near-surface atmosphere in the northern hemisphere of 75 to 80% [*London*, 1957], the authors use a uniform value for $\alpha_{sp,SO4,ion}$ of 8.5 $m^2 g^{-1}$ and apply it globally in their model calculations.

The scattering to mass ratio used in the *Kiehl and Briegleb* [1993] model is estimated from Mie theory coupled with the assumption of a lognormal number size distribution and an aerosol chemical composition of 75% $H_2SO_4$ and 25% $H_2O$. The assumed number size distribution and chemical composition is based on observations of polluted air masses [*Whitby*, 1978; *Palmer and Williams*, 1975; *Weiss et al.*, 1982]. Values of $\alpha_{sp,SO4,ion}$ are allowed to vary with the wavelength of incident light; at 550 nm, $\alpha_{sp,SO4,ion}$ has a value of 5 $m^2 g^{-1}$. The effect of RH on scattering is taken into account by using the same set of observations used by the *Charlson et al.* [1991] model. *Kiehl and Briegleb* [1993] obtain RH from European Centre for Medium-Range Weather Forecasts (ECMWF) temperature and specific humidity data. As a result, $\alpha_{sp,SO4,ion}$ varies regionally with changes in RH.

*Charlson et al.* [1991] use a uniform value of 0.15 for the backscattered fraction, $b$, and apply it globally. This value is based on integrating nephelometer measurements of sulfate haze in eastern North America [*Vanderpol*, 1975]. *Kiehl and Briegleb* [1993] calculate $b$ from an assumed number size distribution and allow it to vary with the wavelength of incident light [*Twomey*, 1977]. Their visible value is 0.1.

Both *Charlson et al.* [1991] and *Kiehl and Briegleb* [1993] use chemical and physical properties which are characteristic of aerosol in urban regions to derive the sulfate scattering to mass ratio and the backscattered fraction for use in their models. As described above, *Charlson et al.* [1991] use uniform values based on direct observations and apply them globally, while *Kiehl and Briegleb* [1993] use values which are calculated from assumed parameters and Mie theory. In addition, *Kiehl and Briegleb* [1993] allow for a wavelength dependence in their calculated optical properties. This difference in approach contributes to a factor of 2 disagreement in the calculated magnitude of the direct radiative effect of sulfate aerosol. This discrepancy indicates a need for observational data over a wide range of geographical regions to improve the agreement between the observed and calculated values and the accuracy in global climate models.

This need for observational data also is indicated by the large uncertainties associated with input parameters currently used in modeling the direct effect [*Penner et al.*, 1994]. For both $\alpha_{sp,SO4,ion}$ and $b$ the estimated uncertainty factor is ±1.4. The uncertainty in these parameters in addition to all other determining variables yields a total uncertainty factor of ±2. These factors are based on a limited set of observations and may not represent the variability of the global atmosphere. As a result, the total uncertainty may be larger.

Measurements from two Pacific Ocean experiments were made with two goals in mind. The first was to determine the regional and temporal variability in aerosol chemical, physical, and optical properties that are relevant to climate forcing. The second was to overdetermine the properties of the aerosol system by coupling measurement and modeling techniques to perform local closure experiments. Closure experiments allow for a test of the internal consistency of the data set and for the indentification of areas where improvements in measurement and/or modeling methods are needed.

The measurements made include the particulate light scattering coefficient, $\sigma_{sp,meas}$, and the backscattering coefficient, $\sigma_{bsp,meas}$; the aerosol number size distribution from 0.02 to 9.6 μm; and the aerosol chemical composition as a function of particle size. The first experiment took place as part of the Pacific Sulfur/Stratus Investigation in April and May of 1991 (PSI 91) at the University of Washington's research site at Cheeka Peak on the northwest tip of Washington State, U. S. The second occurred during the International Global Atmospheric Chemistry Program's Marine Aerosol and Gas Exchange cruise in February and March of 1992 (MAGE 92) which transited the Pacific Ocean from 33°N to 12°S along 140°W. These data are representative of conditions in the least polluted regions of the marine boundary layer and are the opposite extreme from what has served as model input data thus far.

A mass closure experiment was performed in which mass concentrations derived from chemical analysis were compared to those derived from the measured number size distribution to determine how much of the total mass was accounted for by the chemical analysis. To test for scattering closure, Mie theory was coupled with the measured size distributions to calculate $\sigma_{sp,calc}$ and $\sigma_{bsp,calc}$ for all aerosol scattering species present. The calculated values were compared to the measured values to test our ability to adequately model the chemical characteristics of the aerosol and to check for accuracy in the response of the nephelometer.

In addition, Mie calculations were performed to determine (1) the contribution of sulfate aerosol and residual mass to $\sigma_{sp,calc}$ and $\sigma_{bsp,calc}$ where the sulfate aerosol is assumed to consist of nss $SO_4^=$, $NH_4^+$, and associated $H_2O$ at 30% RH; (2) sulfate ion scattering to mass and backscattering to mass ratios, $\alpha_{sp,SO4,ion}$ and $\alpha_{bsp,SO4,ion}$, defined as the sulfate aerosol-apportioned light scattering (backscattering) per unit mass of $SO_4^=$ ion; and (3) sulfate aerosol scattering to mass and backscattering to mass ratios, $\alpha_{sp,SO4,aer}$ and $\alpha_{bsp,SO4,aer}$, defined as the sulfate aerosol-apportioned light scattering (backscattering) per unit mass of $SO_4^=$ aerosol. Finally, the measured values of $b$ and the accumulation mode geometric number mean diameter ($D_{gn}$) and standard deviation ($\sigma_{sg}$) as well as the calculated values of $b$ and $\alpha_{sp,SO4,ion}$ were compared to those used in the model calculations of *Charlson et al.* [1991] and *Kiehl and Briegleb* [1993].

## 2. Methods

### 2.1. Measurements

The location of the measurements made during PSI 91 and MAGE 92 are shown in Figure 1. Cheeka Peak is a mountaintop site (480 m) located 2 km from the Washington coast. During

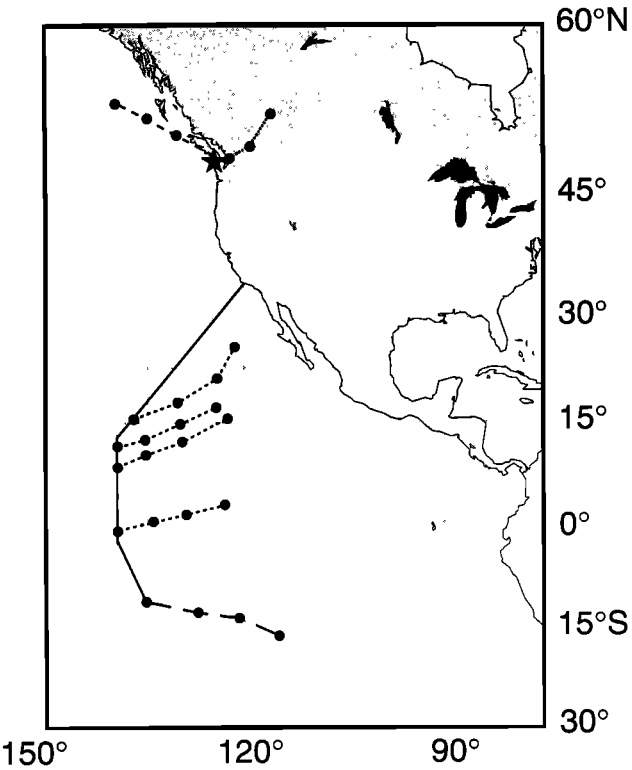


**Figure 1.** Study areas for the Pacific Sulfur/Stratus Investigation of 1991 (PSI 91) and the Marine Aerosol and Gas Exchange cruise of 1992 (MAGE 92). The star indicates the location of Cheeka Peak, while the solid line indicates the MAGE 92 cruise track. Also shown are trajectory analyses calculated by a medium-range forecast (MRF) model. The trajectories are initiated at a fixed height above the ocean surface and are allowed to move vertically using the MRF vertical wind fields. Each circle signifies one day back in time. The dotted line represents samples collected during PSI 91 as the air was coming from aloft and over Canada. The medium-dashed line represents those collected during PSI 91 as air was coming from the west with no subsidence. The short-dashed line represents samples collected during Leg 1 of MAGE 92 as the ship transited from 18°N to 12°S along 140°W and the long-dashed line represents samples collected during the time series station of MAGE 92 at 12°S and 135°W.

PSI 91, sample air for both the chemical and physical aerosol size distribution measurements was drawn from a height of 10 m above ground through a heated tube and dried to a relative humidity of about 30%. Onboard the ship during MAGE 92, air was drawn through a 6-m heated sample inlet and dried to about 30% RH. The top of the inlet was 18 m above the ocean surface and 10 m forward of the ship's stack.

The number size distributions were measured continuously. Samples for the determination of chemical mass size distributions were collected only when the condensation nuclei (CN) count of particles with diameters greater than 0.015 μm was less than 1000 $cm^{-3}$ and the wind speed was greater than 3 m $s^{-1}$. At Cheeka Peak, samples were taken only during periods of local surface westerly flow. Onboard the ship, samples were taken only when the wind direction was forward of the beam.

During PSI 91 and MAGE 92, the number size distribution was measured every 10 min between 0.02 and 0.6 μm with a differential mobility analyzer (DMA) (TSI model 3071; *Liu and Pui* [1975]) and between 0.6 and 9.6 μm with an aerodynamic particle sizer (APS) (TSI model 3300; *Baron* [1986]). A diffusion drier was placed upstream of the inlets to reduce the relative humidity of the sample stream to near 25% at the instrumental temperature.

For the DMA measurements a krypton 85 charge neutralizer (TSI model 3077) was used to produce an equilibrium charge distribution. An impactor with a 50% cutoff diameter of 0.7 μm bounded the upper limit of the aerosol at the inlet and facilitated the inversion algorithm. The RH of the sheath air was less than 25%. A minimum of 1000 particles was counted in each size increment yielding an uncertainty of about 3% for one standard deviation and assuming Poisson counting statistics. The number concentration was corrected for the counting efficiency of the particle counter [*Zang and Liu*, 1991] and diffusion losses in the DMA [*Reineking and Porstendorfer*, 1986]. A Boltzmann-Fuchs equilibrium charge distribution was assumed to be present on the particles analyzed. The number mobility distribution was inverted to a number size distribution using an algorithm similar to that provided by the manufacturer [*Keady et al.*, 1983].

The APS was operated at sample and sheath air flow rates that the manufacturer used for calibration. All flow rates were checked in the field and adjusted to better than 1% on a daily basis. The sheath air was cleaned with filters and charcoal and was at a relative humidity of less than 20%. The APS diameters were converted to geometric diameter by dividing by the square root of the particle density. Densities were obtained from the chemical parameterization that is described in section 2.2. and in further detail by *Marshall* [1994].

A seven-stage multijet cascade impactor [*Berner et al.*, 1979] was used to collect samples for the determination of mass size distributions of $Cl^-$, $Br^-$, $NO_3^-$, nss $SO_4^=$, methanesulfonate or $MSA^-$, $Na^+$, $NH_4^+$, and $K^+$ [*Quinn et al.*, 1993]. Impactor sample information is listed in Table 1 and includes time and location of sample, mixed layer height estimated from radiosonde measurements, RH, surface wind direction, and trajectory. The stages of the impactor had 50% cutoff diameters of 0.125, 0.25, 0.5, 1.0, 2.0, 4.0, and 8.0 μm in aerodynamic particle diameter. For comparison to measurements of the number size distribution, the impactor aerodynamic diameters were converted to geometric diameter by dividing by the square root of an assumed density of 1.7 g $cm^{-3}$. This density was chosen as it approximates that of ammoniated sulfate salts and seasalt at a relative humidity of 30%. The resulting 50% cutoff diameters in terms of geometric diameter are 0.096, 0.19, 0.38, 0.77, 1.5, 3.1, and 6.1 μm. All impactor results are plotted as a function of dry geometric particle diameter at 30% RH.

Tedlar films were used as the collection substrate for the six largest stages and a Millipore Fluoropore filter (1.0-μm pore size) was used for the smallest stage. The Millipore filter has a 99% collection efficiency for particles with diameters larger than 0.035 μm [*Liu and Lee*, 1976]. An impaction stage ($D_p \cong 10$ μm) at the inlet of the impactor was covered with silicone grease to prevent bouncing of large particles onto the downstream stages.

To avoid sample artifacts due to contaminated substrates, films were sonicated in 10% $H_2O_2$ for 30 min, rinsed six times in distilled, deionized water, and dried in an $NH_3$- and $SO_2$-free glove box. All handling of the substrates was done in the glove box. Blank levels were determined by loading the impactor with the substrates and deploying it at the sampling site for the length of a typical sampling period without pulling air through it. Following collection, the blanks were treated in an identical manner as the sample substrates. On average, the $Na^+$ and $SO_4^=$ blanks were 9 and 1% of the sample values, respectively. The $MSA^-$, $NH_4^+$, $K^+$, $Cl^-$, $Br^-$, and $NO_3^-$ blanks were below detection limit.

**Table 1.** PSI 91 and MAGE 92 Impactor Samples

| Sample | Start-Stop Times* | Position | Mixed Layer Height, m | RH, % | Surface Wind Direction | Trajectory† |
|---|---|---|---|---|---|---|
| | | | *PSI 91* | | | |
| 1 | 107.59–108.25 | | 500 ± 57 | 81 ± 16 | 245 ± 7.3 | From Canada; subsidence |
| 2 | 108.85–109.00 | | 475 ± 25 | 99 ± 12 | 279 ± 7.6 | From Canada; subsidence |
| 3 | 111.83–112.88 | | 1070 ± 210 | 95 ± 42 | 261 ± 28 | From Canada; subsidence |
| 4 | 113.38–115.27 | | mixed through FT | 94 ± 73 | 233 ± 31 | From Canada and west; subsidence |
| 5 | 115.35–116.10 | | 1300 ± 103 | 84 ± 74 | 246 ± 54 | From NW |
| 6 | 116.75–118.11 | | 1380 | 89 ± 54 | 260 ± 74 | From NW |
| 7 | 118.58–119.18 | | 930 ± 630 | 85 ± 38 | 272 ± 78 | From west |
| | | | *MAGE 92* | | | |
| 1 | 56.733–57.138 | 18.99°N, 133.63°W | 1900 | 56 ± 4.5 | 77 ± 9.5 | From NE |
| 2 | 57.267–58.121 | 16.04°N, 136.22°W | 1400 | 62 ± 5.7 | 78 ± 11 | From NE |
| 3 | 58.223–58.975 | 10.24°N, 139.47°W | 1800 | 85 ± 1.9 | 50 ± 14 | From NE |
| 4 | 59.296–60.158 | 6.63°N, 139.99°W | 2400 | 73 ± 3.6 | 54 ± 7.4 | From NE |
| 5 | 60.279–61.146 | 1.78°N, 140.00°W | 3300 | 81 ± 2.5 | 65 ± 7.9 | From NE |
| 6 | 61.246–62.138 | –2.70°N, 139.92°W | 3400 | 82 ± 6.2 | 90 ± 12 | From east |
| 7 | 64.233–65.146 | –11.98°N, 135.12°W | 1600 | 74 ± 2.9 | 110 ± 12 | From E/SE |
| 8 | 65.221–66.129 | –12.05°N, 135.01°W | 2300 | 72 ± 1.3 | 99 ± 13 | From E/SE |
| 9 | 67.208–68.150 | –12.29°N, 134.50°W | 2100 | 73 ± 1.1 | 95 ± 9.04 | From E/SE |
| 10 | 68.208–69.150 | –12.43°N, 134.32°W | 2300 | 74 ± 1.6 | 88 ± 16 | From E/SE |
| 11 | 69.592–70.867 | –11.56°N, 135.20°W | 2000 | 76 ± 1.8 | 87 ± 15 | From east |

RH, relative humidity; FT, free troposphere
*PSI 91 times are LT; MAGE 92 times are UT.
†Unless noted otherwise, trajectories indicated no subsidence.

The time period of impactor sampling ranged from 12 to 24 hours. After sample collection, the material on the films and filter was extracted by first wetting with 1 ml of methanol and then adding 5 ml of distilled deionized water and sonicating for 15 min. Extracts were analyzed by ion chromatography. The cation analysis of $Na^+$, $NH_4^+$, and $K^+$ was performed with a Dionex CS-1 column, 0.5-m*M* HCl eluent, and 68-m*M* tetramethylammonium hydroxide monohydrate regenerant. Sulfate analysis was done with a Dionex AS-4A column, 0.75-m*M* $NaHCO_3$/2.0-m*M* $Na_2CO_3$ eluent, and 12.6-m*M* $H_2SO_4$ regenerant. $MSA^-$ analysis was performed with a Dionex AS-4 column, a 5-m*M* NaOH mobile phase to elute the weak organic acids followed by 100-m*M* NaOH to elute the stronger acids, and 12.6-m*M* $H_2SO_4$ regenerant. Nonseasalt $SO_4^=$ concentrations were calculated from $Na^+$ concentrations and the molar ratio of sulfate to sodium in seawater of 0.0603 [*Holland*, 1978].

For both PSI 91 and MAGE 92, sample air for the measurement of $\sigma_{sp,meas}$ and $\sigma_{bsp,meas}$ was drawn from the same location as that for the size distribution measurements and dried to a relative humidity of 30%. Scattering measurements were made at a wavelength of 0.55 μm with an integrating nephelometer [*Charlson et al.*, 1967] over a scattering angle, θ, where $8° \le \theta \le 168°$. The hemispheric backscattered fraction, *b*, was taken as the ratio $\sigma_{bsp}/\sigma_{sp}$ where $\sigma_{bsp}$ was determined from an integral over $90° \le \theta \le 168°$. Every 3 to 4 days the nephelometer was calibrated with $CO_2$ and zeroed with particle-free air.

Ancillary measurements included surface temperature, dew point, wind speed, and wind direction. Air mass back trajectories were calculated using the hybrid single-particle Lagrangian integrated trajectories (HY-SPLIT) model based on wind fields generated by the medium range forecast (MRF) model [*Draxler*, 1992]. For Cheeka Peak the trajectories were calculated such that they terminated at a fixed height of 480 m above the ocean surface. For the shipboard calculations the trajectories were terminated at the ocean surface.

### 2.2. Model Calculations

Mie theory was applied to the measured number size distributions to predict the scattering and backscattering coefficients measured by the nephelometer. The model calculations are described briefly here and in greater detail in *Marshall* [1994]. The scattered intensity function, $|S(\theta,x,n)|$, was integrated over zenith angle θ to derive the scattering and backscattering efficiencies, $Q_{sp}$ and $Q_{bsp}$, respectively, as follows

$$Q_{sp;bsp} = \frac{1}{x^2}\int |S(\theta,x,n)|^2 \sin\theta d\theta \quad (4)$$

where the sinθ term is specific to lambertian illumination of the particle, *n* is the refractive index, and *x* is the size parameter defined as

$$x = \frac{\pi D_p}{\lambda} \quad (5)$$

where $D_p$ is the geometric diameter of the particle and the particle is assumed to be spherical. The angles of integration were 0° to 180° for the total scattering efficiency and 90° to 180° for the hemispheric backscattering efficiency.

The scattering (backscattering) efficiency was then integrated over the measured number size distribution to yield the scatter-

ing (backscattering) coefficient using

$$\sigma_{sp;bsp} = \int Q_{sp,bsp}(D_p,\lambda,n)\pi D_p^2 \frac{dN}{d\log D_p} d\log D_p \quad (6)$$

Two sets of Mie calculations of the backscattering coefficient were performed. The first was an unmodified calculation that is described by (6). The second was modified to account for nonideal integration and illumination functions of the nephelometer used in the field experiments. To model the instrument response, the angular limits of integration were adjusted to those defined by the truncation angles of the nephelometer and the cutoff angles of the backscatter shutter. The effect of nonlambertian illumination by the light source was estimated by replacing the sinθ term in (4) with an angular sensitivity function taken from a nephelometer calibration by *Heintzenberg* [1978]. Integrating the modified values of the backscattering efficiency over the number size distribution resulted in an estimate of the backscattering coefficient, $\sigma_{nbsp,calc}$, for the nephelometer.

The Mie calculations were performed at a wavelength of 0.55 μm corresponding to the central value of the nephelometer wavelength response. Sensitivity calculations using a gaussian wavelength response centered at 0.55 μm yielded scattering coefficients and backscattering coefficients less than 2 to 4% and 1 to 3% greater than the single wavelength calculations, respectively.

The number size distributions used in (6) were obtained by averaging the measured DMA and APS data over times corresponding to MAGE 92 impactor samples 1, 2, 3, 9, 10, and 11 and all of the PSI 91 impactor samples as the complete number size distribution was available for these periods. For the Mie calculations the water mass associated with the nss $SO_4^=$ aerosol component was assumed to be equivalent to that associated with $H_2SO_4$ at 30% RH. This RH corresponds to the operating conditions of the nephelometer and sizing instrumentation.

The particles were assumed to be homogeneous spheres distributed as an external mixture of two components, nss $SO_4^=$ and all additional analyzed mass, referred to as the residual mass. The residual mass was composed of seasalt ions, $NO_3^-$, and $MSA^-$ and was estimated for each impactor stage by summing the measured ion concentrations as follows

$$m_{residual} = m_{Na} + m_{Mg} + m_{Ca} + m_K + m_{Cl} + m_{seasalt\ SO4} + m_{NO3} + m_{MSA} \quad (7)$$

In cases where one or more of the seasalt ion concentrations were unavailable, a concentration was calculated using the molar ratio of the ion to $Na^+$ in seawater [*Holland*, 1978]. Water was not included in the calculation of the residual mass. The residual mass was assigned a constant refractive index of $1.5–10^{-8}$i [*Kent et al.*, 1983] and a density of 1.9 g $cm^{-3}$ corresponding to that of seasalt.

To determine the density and refractive index of the sulfate component, it was partitioned into the three species, $H_2SO_4$, $NH_4HSO_4$, and $(NH_4)_2SO_4$, according to the measured $NH_4^+$ to nss $SO_4^=$ molar ratio for each impactor stage. The density of the mixture was derived from solution data for $H_2SO_4$ [*Bray*, 1970], $NH_4HSO_4$ [*Tang and Munkelwitz*, 1994], and $(NH_4)_2SO_4$ [*Tang and Munkelwitz*, 1991]. The imaginary refractive index of the sulfate component was given a constant value of $10^{-7}$i [*Kent et al.*, 1983]. The real portion of the refractive index was estimated using the molar refraction method of *Stelson* [1990] and values of the electrolyte molar refraction from *Tang and Munkelwitz* [1994].

Apportionment calculations were performed to partition the calculated scattering and backscattering between the nonseasalt sulfate aerosol component and the residual component. The number concentration in each impactor size bin was partitioned between the two components using a volume weighting derived from the measured mass size distributions and calculated density values. The sulfate number size distribution was estimated from

$$\left(\frac{dN}{d\log D_p}\right)_{SO4,aer} = \left(\frac{m_{SO4,aer}\rho_{SO4,aer}}{m_{SO4,aer}\rho_{SO4,aer} + m_{residual}\rho_{residual}}\right)\frac{dN}{d\log D_p} \quad (8)$$

where $m_{SO4,aer}$ and $m_{residual}$ are the sulfate aerosol and residual masses and $\rho_{SO4,aer}$ and $\rho_{residual}$ are the sulfate aerosol and residual densities. The residual number size distribution was estimated similarly. Scattering and backscattering coefficients were calculated by substituting these values of $(dN/d\log D_P)_{SO4,aer}$ and $(dN/d\log D_P)_{residual}$ into (6).

The light scattering coefficients and the chemical mass size distributions can be combined to yield the scattering to mass ratio, $\alpha_{sp}$, defined as

$$\alpha_{sp} = \frac{\sigma_{sp}}{m_p} \quad (9)$$

where $\sigma_{sp}$ is a result of all aerosol scattering species present and $m_p$ is the aerosol mass per unit volume of air. If the aerosol is partitioned into chemical components, scattering to mass ratios can be defined for each component as the scattering by component $j$, $\sigma_{sp,j}$, divided by the mass of component $j$ per unit volume of air, $m_j$,

$$\alpha_{sp,j} = \frac{\sigma_{sp,j}}{m_j} \quad (10)$$

For the sulfate aerosol component ($SO_4^=$,aer), $\alpha_{sp,SO4,aer}$ would be

$$\alpha_{sp,SO4,aer} = \frac{\sigma_{sp,SO4,aer}}{m_{SO4,aer}} \quad (11)$$

If the total mass of component $j$ is unknown, an individual species, ind$j$, can be used as an indicator for that component such that

$$\alpha_{sp,indj} = \frac{\sigma_{sp,j}}{m_{indj}} \quad (12)$$

where $\alpha_{sp,indj}$ is the scattering to mass ratio of the single species, and $m_{indj}$ is the mass concentration of that species. An example of an indicator is the use of nss $SO_4^=$ to represent the complete sulfate aerosol containing nss $SO_4^=$, $NH_4^+$, and $H_2O$ such that $\alpha_{sp,SO4,ion}$ is given by

$$\alpha_{sp,SO4,ion} = \frac{\sigma_{sp,SO4,aer}}{m_{SO4,ion}} \quad (13)$$

The backscattering to mass ratio, $\alpha_{bsp,j}$, can be calculated by substituting $\sigma_{bsp,j}$ for $\sigma_{sp,j}$ into (10) and (12).

There are uncertainties associated with the measurements which will contribute to the uncertainty of the predicted scattering and backscattering values. The chemical composition of the aerosol was not fully characterized so that the index of refraction

and density as a function of particle size are known only approximately. In addition, the illumination and angular integration characteristics of the nephelometer were approximated in the model. These approximations will affect the accuracy of the calculated scattering and backscattering coefficients.

An error propagation analysis was carried out to estimate the effects of these uncertainties on the calculated scattering. A detailed description of this analysis is given in *Marshall* [1994]. The uncertainties considered include statistical fluctuation in the average number concentration, instrumental errors in particle sizing and counting due to flow irregularities in the DMA and APS, and uncertainties in the density parameterizations and assumed RH. These uncertainties result in an estimated accuracy of about +20% and −13% in the calculation of $\sigma_{sp,calc}$, $\sigma_{bsp,calc}$, and $\sigma_{nbsp,calc}$.

## 3. Results of Measurements

### 3.1. Calculated Air Mass Trajectories

The air masses sampled at Cheeka Peak during PSI 91 were divided into two categories based on the calculated air mass trajectories. From day (local standard time) 107.59 to 115.27, trajectories indicated that the sample air had originated at the surface, was mixed into the free troposphere, then subsided from aloft and passed over Canada in the 2 or 3 days prior to sampling. From day (local) 115.35 to 119.18, trajectories showed no evidence of subsidence and that the air had come from a northwesterly to westerly direction passing over the ocean surface for several days prior to being sampled. A typical trajectory from each time period is shown in Figure 1.

Trajectories for the MAGE 92 cruise track also are shown in Figure 1. Between about 20°N and 3°S the sample air had come from a northeasterly to easterly direction along the surface and had spent at least 3 days over the eastern Pacific Ocean. Air masses sampled between 3° and 12°S had come from a southeasterly direction along the surface and also had spent several days over the eastern Pacific. The samples were divided into two groups. The first contains the samples that were collected during Leg 1 as the ship traveled from 18°N to 12°S along 140°W. The second consists of samples collected during a 7-day time series station from day 64.6 to 70 (GMT) at 12°S and 135°W.

### 3.2. Measured Size Distributions

**3.2.1. Number and Volume Size Distributions.** The number size distributions measured continuously during PSI 91 and MAGE 92 were averaged over the collection time periods of the impactor samples. Volume size distributions were calculated from the averaged number size distributions assuming spherical particles. The number and volume size distributions are shown in Figures 2 and 3 for PSI 91 and MAGE 92, respectively. During both PSI 91 and MAGE 92 the size distributions revealed pronounced Aitken, accumulation, and coarse modes. The geometric number mean diameter ($D_{gn}$), geometric standard deviation ($\sigma_{sg}$) and total number ($N$) of these modes for the average number size distributions are listed in Table 2.

**3.2.2. Mass Size Distributions.** Information about the impactor samples is listed in Table 1 and includes time and location of sample collection, mixed layer height, RH, surface wind direction, and trajectory. Mass size distributions of $Na^+$, $NH_4^+$, $K^+$, $Cl^-$, $Br^-$, $NO_3^-$, nss $SO_4^=$, and $MSA^-$ were measured during both PSI 91 and MAGE 92. For PSI 91, mass size

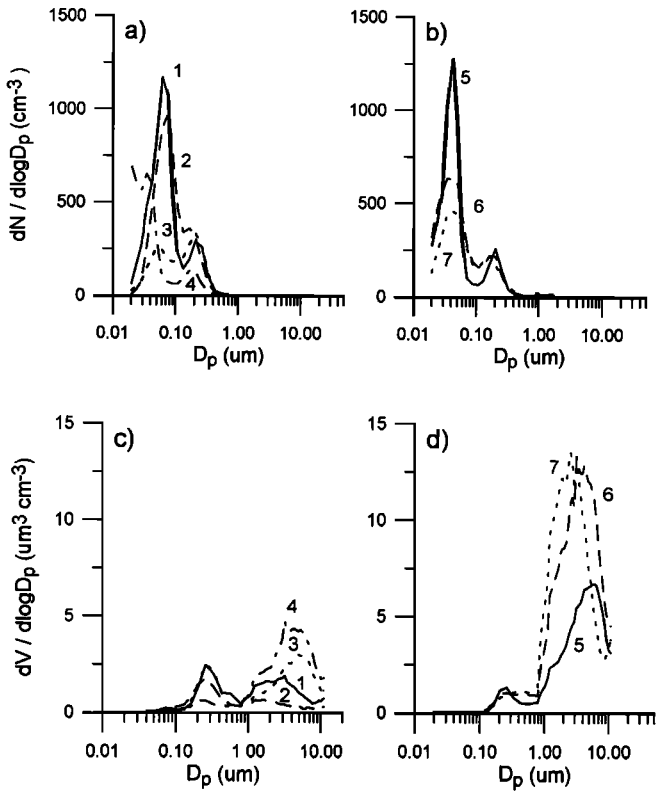


**Figure 2.** Particle number and volume size distributions measured during PSI 91 at 30% RH. Number size distributions were averaged over the time period of the corresponding impactor sample. Volume size distributions were calculated from the measured number distribution. Number of the corresponding impactor sample is indicated. Number size distributions collected (a) as air was coming from aloft and over Canada and (b) during westerly airflow. Volume size distributions collected (c) as air was coming from aloft and over Canada and (d) during westerly airflow.

distributions of $Na^+$, nss $SO_4^=$, $MSA^-$, and $NH_4^+$ were averaged over the time period of northerly winds (number of samples, $n$ = 4) and westerly winds ($n$ = 3) (Figure 4). MAGE 92 samples were averaged over Leg 1 ($n$ = 6) and the time series station ($n$ = 7) (Figure 5). The large standard deviations for both experiments indicate that there was a high degree of spatial or temporal variability in the concentration of these species as a function of size. This variability can be seen more clearly in Figures 6 and 7 where each measured nss $SO_4^=$ and $Na^+$ mass size distribution is plotted for PSI 91 and MAGE 92, respectively.

During PSI 91, as air was coming from aloft and over Canada, the nss $SO_4^=$ and $MSA^-$ mass size distributions did not have a pronounced bimodal character between the accumulation and coarse modes. Only 11 ± 6% of the nss $SO_4^=$ and 5.9 ± 4.8% of the $MSA^-$ occurred in coarse mode particles. During periods of westerly on-shore flow, the volume and $Na^+$ concentration in the coarse mode increased. In addition, the nss $SO_4^=$ and $MSA^-$ size distributions were more bimodal with 25 ± 10% of the nss $SO_4^=$ and 19 ± 14% of the $MSA^-$ in the supermicron fraction. This corresponding increase in coarse mode $Na^+$, nss $SO_4^=$, and $MSA^-$ mass suggests that as more coarse mode surface area became available, gas phase MSA, $SO_2$, and/or $H_2SO_4$ condensed upon the basic seasalt particles. $NH_4^+$ occurred primarily in the submicron fraction throughout the experiment; it was

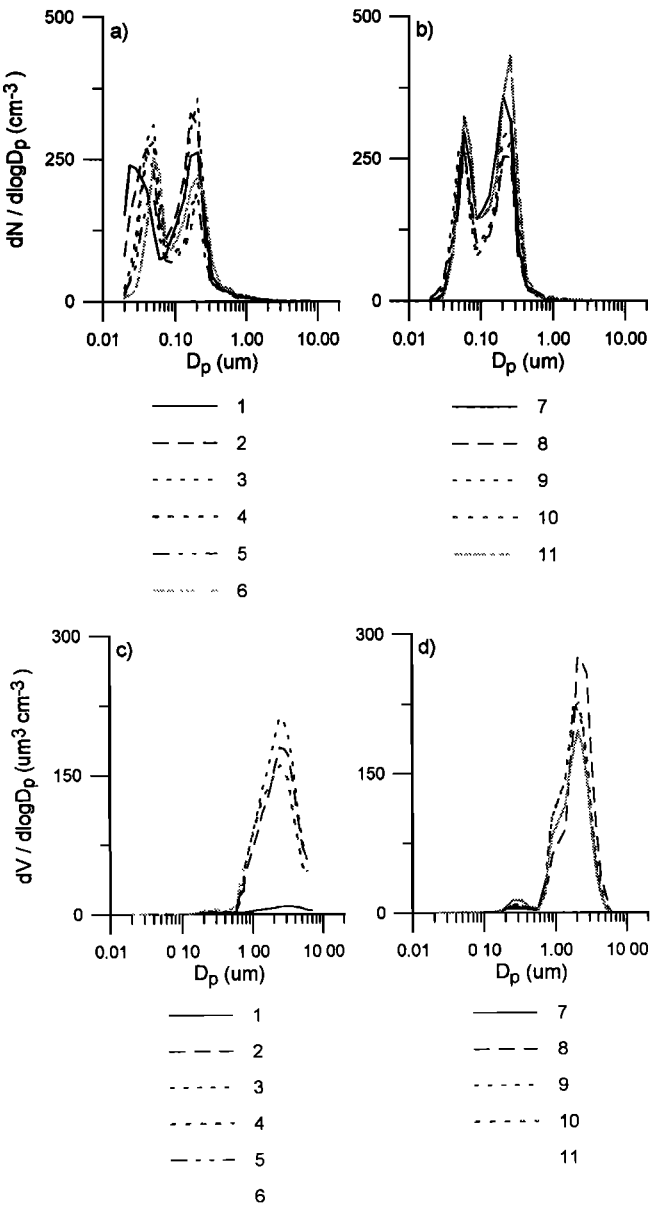


**Figure 3.** Particle number and volume size distributions measured during MAGE 92 at 30% RH. Number size distributions were averaged over the time period of the corresponding impactor sample. Volume size distributions were calculated from the measured number distribution. Number of the corresponding impactor sample is indicated. Number size distributions collected (a) during Leg 1 and (b) during the time series station. Volume size distributions collected (c) during Leg 1 and (d) during the time series station.

detected in the supermicron mode in only two out of seven samples collected. The submicron maximum in the nss $SO_4^=$, $MSA^-$, and $NH_4^+$ size distributions occurred at less than 0.13 μm or between 0.13 and 0.21 μm (at 30% RH).

During Leg 1 and the time series stations of MAGE 92, the majority of the nss $SO_4^=$ mass was found in the submicron fraction with only 11 ± 10% in the supermicron mode. The $MSA^-$ size distributions were more bimodal with 41 ± 12% of the mass in the supermicron fraction. No $NH_4^+$ was detected in the coarse mode throughout MAGE 92. The submicron maximum in the nss $SO_4^=$, $MSA^-$, and $NH_4^+$ size distributions occurred between 0.13 and 0.21 μm (at 30% RH).

**Table 2.** Modal Values of the Average Number Size Distributions Measured During PSI 91 and MAGE 92

| Mode | PSI 91 | MAGE 92 |
|---|---|---|
| | $D_{gn}$, μm | |
| Aitken | 0.047 ± 0.014 | 0.049 ± 0.013 |
| Accumulation | 0.19 ± 0.02 | 0.19 ± 0.027 |
| Coarse | 0.47 ± 0.11 | 0.86 ± 0.43 |
| | $\sigma_{sg}$ | |
| Aitken | 1.5 ± 0.11 | 1.4 ± 0.12 |
| Accumulation | 1.4 ± 0.053 | 1.4 ± 0.06 |
| Coarse | 2.0 ± 0.095 | 1.8 ± 0.305 |
| | $N$, $cm^{-3}$ | |
| Aitken | 350 ± 120 | 102 ± 21 |
| Accumulation | 86 ± 24 | 114 ± 14 |
| Coarse | 5.6 ± 4.2 | 5.7 ± 4.7 |

The Aitken mode includes particles with geometric diameters less than 0.1 μm, the accumulation mode includes particles between 0.1 and 0.8 μm, and the coarse mode includes all particles between 0.8 and 10 μm.

$D_{gn}$, geometric number mean diameter; $\sigma_{sg}$, geometric standard deviation; $N$, total number concentration.

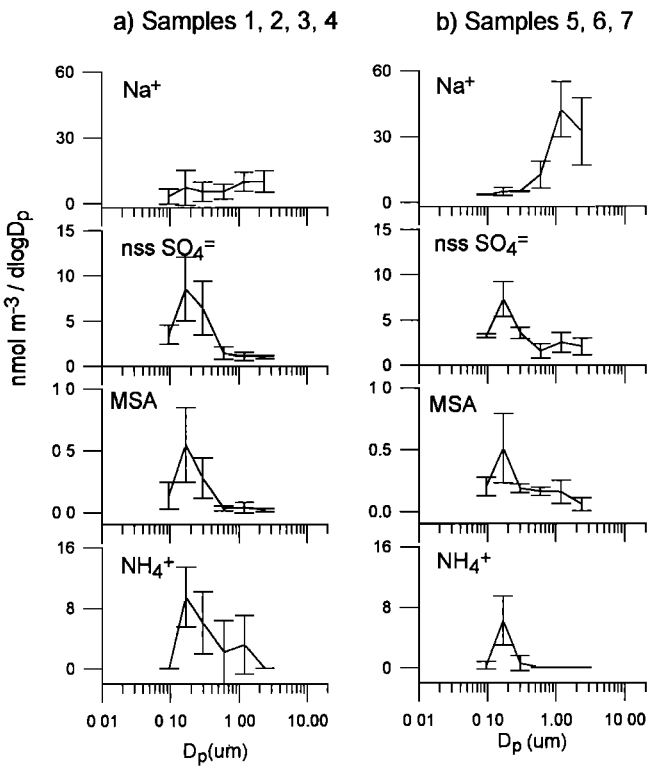


**Figure 4.** Average mass size distribution of $Na^+$, nonseasalt (nss) $SO_4^=$, methanesulfonate ($MSA^-$), and $NH_4^+$ collected during PSI 91 at 30% RH. Mass concentration is plotted as a function of geometric diameter. Average distribution of (a) samples 1, 2, 3, and 4 as air was coming from aloft and over Canada and (b) samples 5, 6, and 7 during westerly air flow. Vertical bars represent the standard deviation of the data.

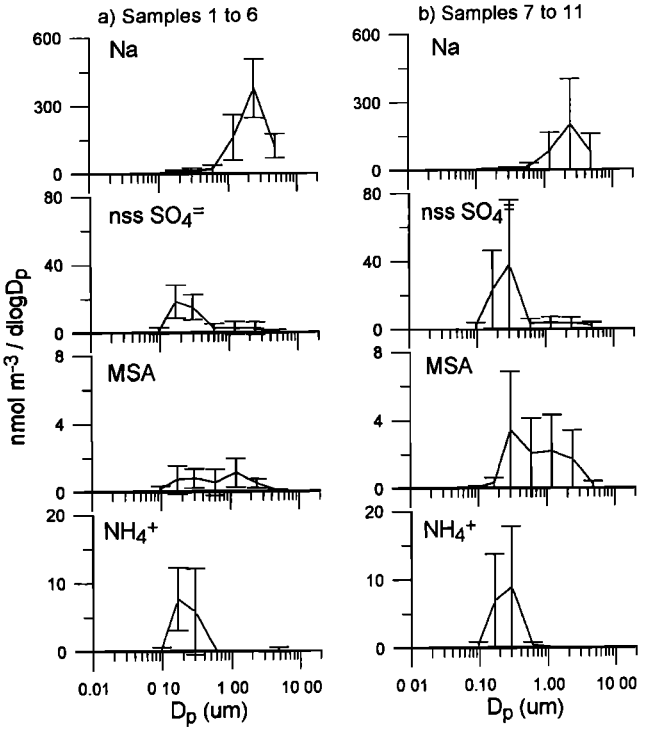


**Figure 5.** Average mass size distribution of $Na^+$, nss $SO_4^=$, $MSA^-$, and $NH_4^+$ collected during MAGE 92 at 30% RH. Mass concentration is plotted as a function of geometric diameter. Average distribution of (a) samples 1 through 6 collected during Leg 1 and (b) samples 7 through 11 collected during the time series station. Vertical bars represent the standard deviation of the data.

### 3.3. Measured Light Scattering and Backscattering Coefficients

The light scattering and backscattering coefficients were measured for all particles with diameters less than about 10 μm. These values were averaged over the time periods of the impactor samples. During PSI 91, $\sigma_{sp,meas}$ ranged from 3.7 to $14 \times 10^{-6}$ $m^{-1}$ (Figure 8). As the sampled air was coming from aloft and over Canada (samples 1 through 4), $\sigma_{sp,meas}$ had an average and standard deviation of $5.5 \pm 1.5 \times 10^{-6}$ $m^{-1}$. During conditions of westerly on-shore flow (samples 5 through 7), both the volume concentration and the $Na^+$ concentration in the coarse mode increased. Correspondingly, $\sigma_{sp,meas}$ rose to $10.4 \pm 4.2 \times 10^{-6}$ $m^{-1}$. Throughout the experiment, $\sigma_{bsp,meas}$ ranged between 0.63 and $1.4 \times 10^{-6}$ $m^{-1}$ resulting in a backscattered fraction of 0.12 to 0.2 with an average and standard deviation of $0.15 \pm 0.009$. During MAGE 92 the measured $\sigma_{sp,meas}$ and $\sigma_{bsp,meas}$ were fairly constant throughout Leg 1 and the time series station (Figures 9 and 10, respectively). Values of $\sigma_{sp,meas}$ ranged from 9.8 to $15 \times 10^{-6}$ $m^{-1}$ and $\sigma_{bsp,meas}$ from 1.5 to $2.2 \times 10^{-6}$ $m^{-1}$. The backscattered fraction averaged $0.15 \pm 0.009$.

## 4. Results of Model Calculations

### 4.1. Mass Closure

The mass concentrations of the impactor samples determined from ion chromatography (IC) analysis were compared to the mass concentrations calculated from the averaged number size distributions to test for consistency between these two independent data sets. The results are shown in Figures 11a and 11b. The number-derived mass was calculated from the measured number size distribution and an assumed density, independent of particle size, of either 1.4 or 1.9 g $cm^{-3}$. This density range encompasses that of nss $SO_4^=$ and seasalt aerosol. Both the mass size distributions and the number size distributions were determined near 30% RH.

For PSI 91 (Figure 11a) the IC-analyzed mass was consistently lower than the number-derived mass; in six of the seven samples the IC mass only accounted for 42 to 62% of the number-derived mass. For two of the six MAGE 92 samples (Figure 11b), the IC-analyzed mass was larger than the number-derived mass (M1 and M3). For the remaining four, the two estimates of mass agreed within ±25% of each other.

Sampling and instrumental uncertainties may contribute to the disagreement between the IC- and number-derived mass. These uncertainties include collection efficiencies of the impactor stages (±2 to 27% [*Wang and John*, 1988]) and counting errors associated with the number sizing equipment. An incomplete characterization of the aerosol chemical composition by IC also would lead to a difference between the number- and IC-derived mass. The low values of IC-derived mass relative to the number-derived mass for all of the PSI 91 samples suggests that chemical species were present that were not detected by IC. These could include mineral dust, organics, and elemental carbon. The unaccounted for mass fraction was not significantly greater for continental versus ocean trajectories during PSI 91, however. It is possible that different chemical

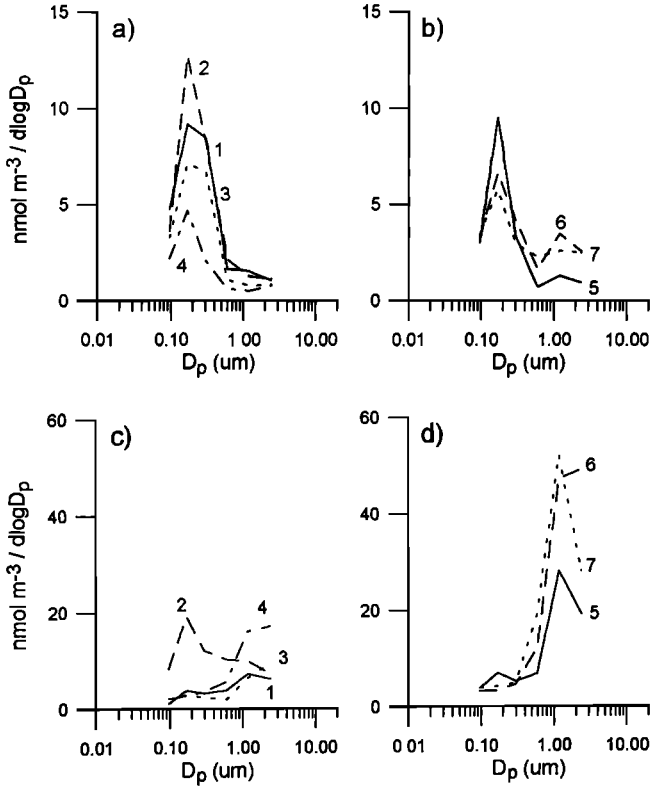


**Figure 6.** Individual mass size distributions collected during PSI 91 at 30% RH. Sample numbers are indicated. Mass concentration is plotted as a function of geometric diameter. Size distributions of nss $SO_4^=$ collected (a) as air was coming from aloft and over Canada and (b) during westerly air flow. Size distributions of $Na^+$ collected (c) as air was coming from aloft and over Canada and (d) during westerly air flow.

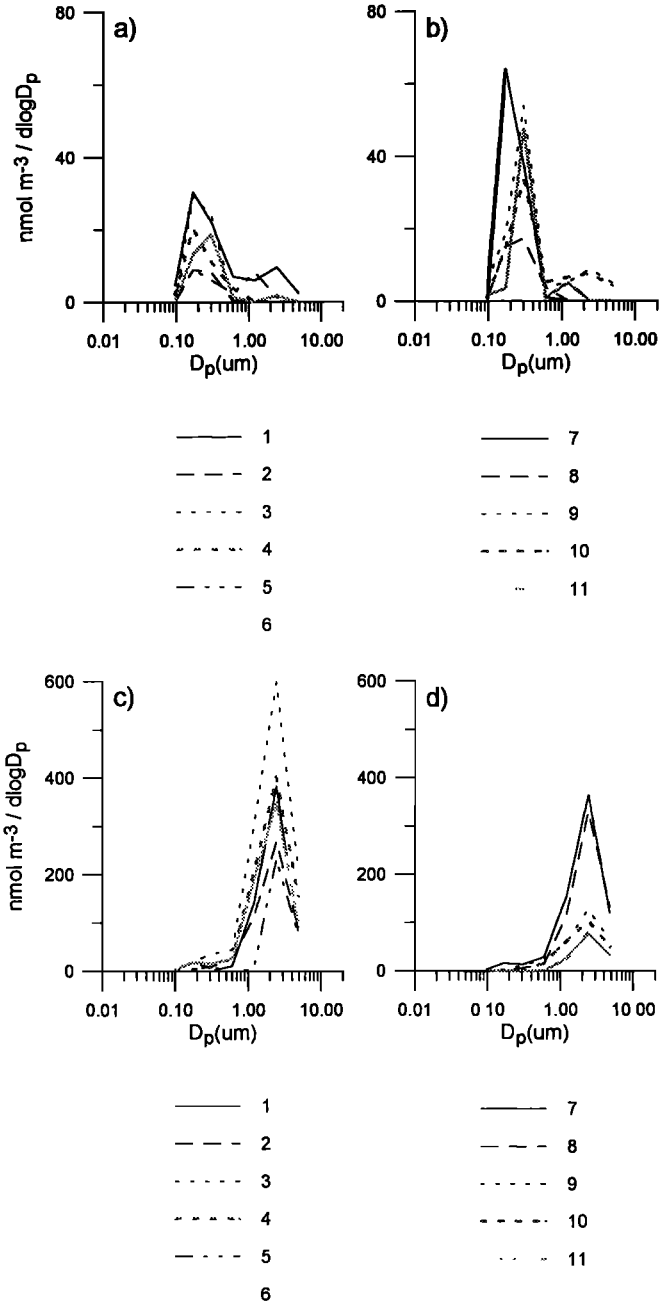


**Figure 7.** Individual mass size distributions collected during MAGE 92 at 30% RH. Mass concentration is plotted as a function of geometric diameter. Sample numbers are indicated. Size distributions of nss $SO_4^=$ collected (a) during Leg 1 and (b) during the time series station. Size distributions of $Na^+$ collected (c) during Leg 1 and (d) during the time series station.

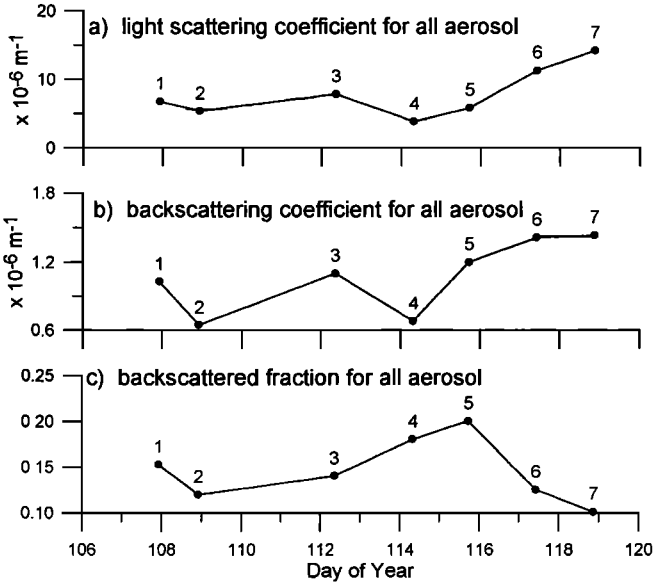


**Figure 8.** Nephelometer measurements of (a) light scattering, (b) backscattering, and (c) the backscattered fraction during PSI 91 as a function of day of year (local). Number of the corresponding impactor sample is indicated.

species with comparable scattering characteristics contributed similary to this mass fraction for the two types of trajectories.

In addition, different particle collection efficiencies for the impactor and the sizing equipment would lead to a discrepancy between the two estimates of mass. This may have contributed to the discrepancy for the MAGE 92 samples as the inlet configurations for the sizing equipment and the impactor were different. Sample air flow into the impactors required only one shallow bend in the inlet tubing. Flow into the DMA and APS required two 90° bends.

The lack of agreement between the number- and IC-derived mass for all of the PSI 91 samples and two of the MAGE 92 samples indicates that several aspects of the sampling procedure need to be improved upon in order for closure to be achieved. A complete characterization of the aerosol chemical composition as a function of particle size would make the chemically derived and number-derived mass more directly comparable. A more complete chemical analysis would include determining the mass concentrations of organic species, elemental carbon, trace metals, and mineral dust. Gravimetric analysis of the mass collected on each impactor stage would be useful as it would provide a third independent measure of total aerosol mass. In

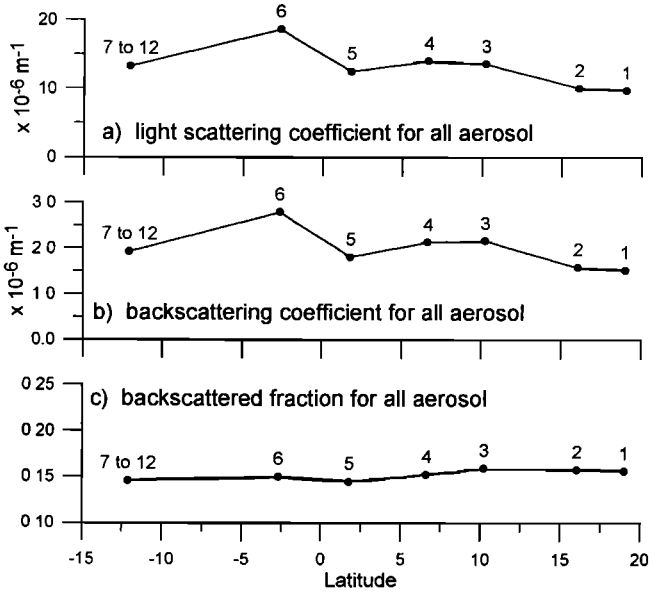


**Figure 9.** Nephelometer measurements of (a) light scattering, (b) backscattering, and (c) the backscattered fraction during Leg 1 of MAGE 92 as a function of latitude. Number of the corresponding impactor sample is indicated.

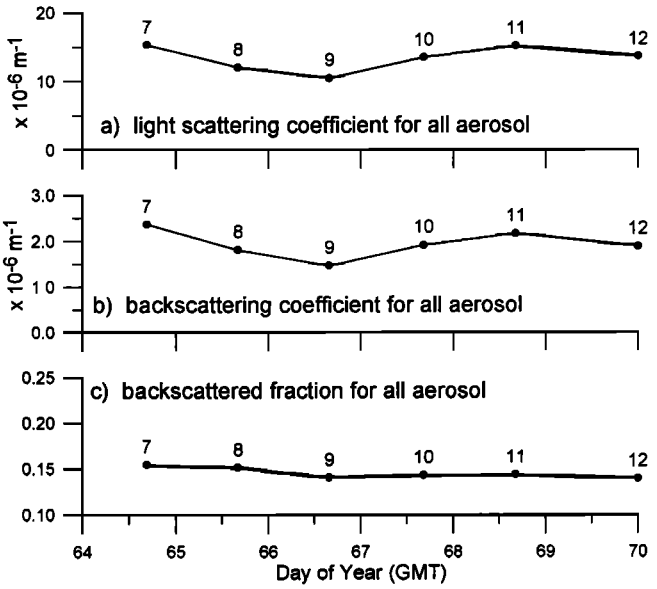


**Figure 10.** Nephelometer measurements of (a) light scattering, (b) backscattering, and (c) the backscattered fraction during the MAGE 92 time series station at 12°S and 135°W as a function of day of year (GMT). Number of the corresponding impactor sample is indicated.

addition, the inlet configuration for the impactor, sizing equipment, and nephelometer should be the same.

### 4.2. Scattering Closure

The calculated and measured values of the scattering and backscattering coefficients were compared to determine if the aerosol chemical characteristics were modeled adequately and the degree of accuracy of the nephelometer response (Figures 12 and 13, respectively, and Table 3). The error bars shown in the Figures represent the maximum and minimum values of the calculated coefficients if the following sources of error are taken into account: statistical fluctuation in the average number concentration, instrumental errors in particle sizing and counting due to flow irregularities in the DMA and APS, and uncertainties in the density parameterizations and assumed RH [*Marshall*, 1994].

The average and standard deviation of the calculated scattering coefficient, $\sigma_{sp,calc}$, was $10.3 \pm 4.0 \times 10^{-6}$ m$^{-1}$ and the average and standard deviation of the measured value was $10.0 \pm 3.9 \times 10^{-6}$ m$^{-1}$. The mean value of $\sigma_{sp,calc}$ was 3% higher than the mean measured value with a variance around the mean of 14%. This is within the uncertainty of the calculations. The good agreement between $\sigma_{sp,calc}$ and $\sigma_{sp,meas}$ indicates that the scattering characteristics of the aerosol were parameterized accurately by the model and that closure was achieved for this set of measurements.

The average and standard deviation of the calculated value of the backscattering coefficient, $\sigma_{bsp,calc}$, was $0.98 \pm 0.35 \times 10^{-6}$ m$^{-1}$, while the average and standard deviation of the measured value, $\sigma_{bsp,meas}$, was $1.4 \pm 0.51 \times 10^{-6}$ m$^{-1}$. Hence the mean calculated value was about 40% lower than the mean measured value. In an attempt to improve the agreement between the calculated and measured backscattering values, a second set of Mie calculations was performed which was modified to account for nonideal nephelometer integration and illumination functions (see section 2.2). As shown in Figure 13, the backscattering

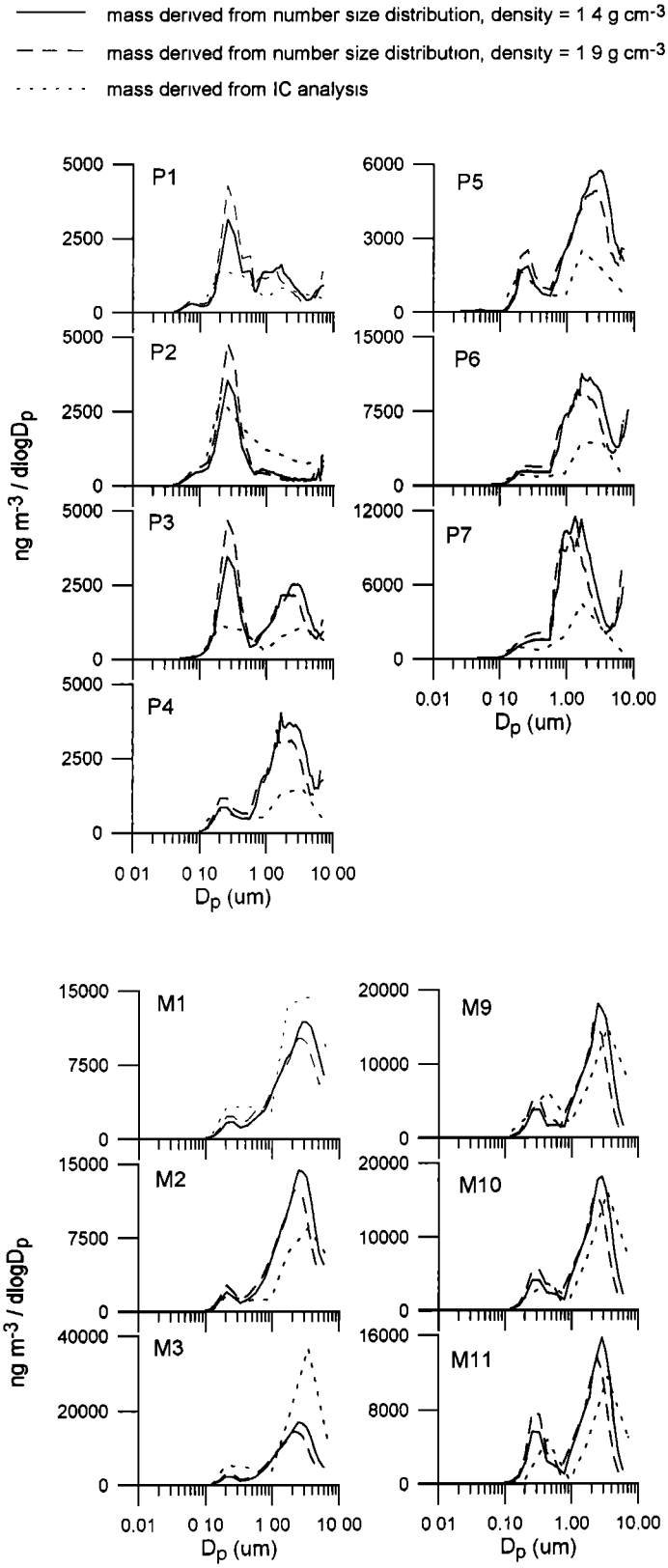


**Figure 11.** Three estimates of the mass size distribution are shown: one is based on the measured number size distribution and the assumption of a single component aerosol with a density of 1.4 g cm$^{-3}$, the second is based on the measured number size distribution and the assumption of a single component aerosol with a density of 1.9 g cm$^{-3}$, and the third is based on the ion chromatography (IC)-analyzed mass size distributions for (a) PSI 91 and (b) MAGE 92. Impactor sample numbers are indicated.

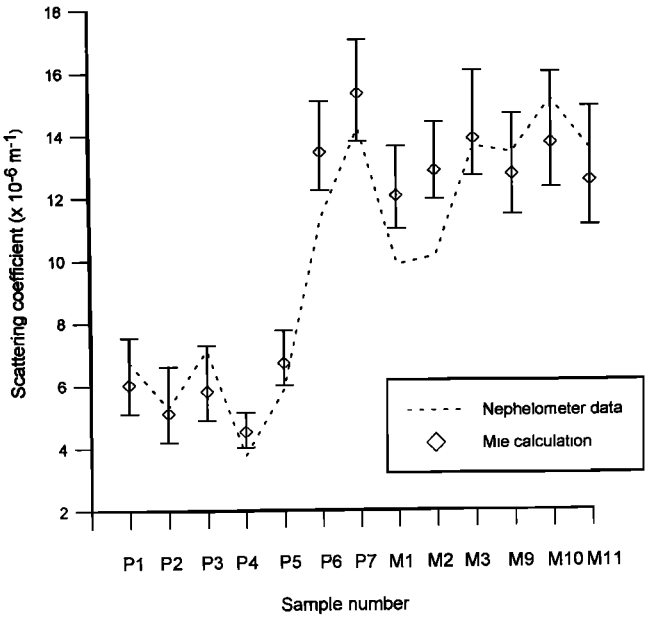


**Figure 12.** Comparison of measured and calculated values of the scattering coefficient. The error bars represent the maximum and minimum values of the coefficients derived from the Mie calculations if all sources of uncertainty are taken into account (see section 2.2). Impactor sample numbers are indicated where P represents PSI 91 and M represents MAGE 92.

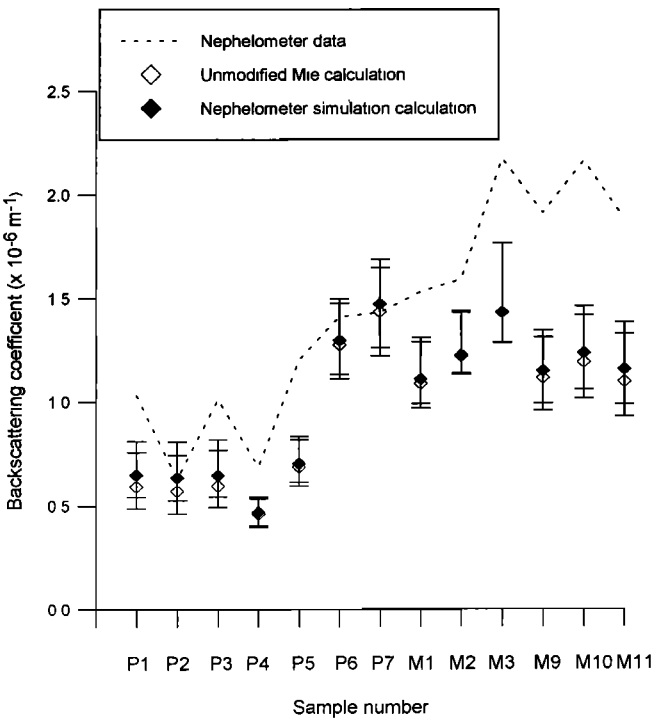


**Figure 13.** Comparison of measured and calculated values of the backscattering coefficient. Two Mie calculations were performed with one being unmodified and one including a simulation of the nephelometer properties. The error bars represent the maximum and minimum values of the coefficients derived from the base case calculation if all sources of uncertainty are taken into account. Impactor sample numbers are indicated where P represents PSI 91 and M represents MAGE 92.

coefficients derived from this nephelometer simulation, $\sigma_{nbsp,calc}$, were not significantly different from those based on the unmodified Mie calculation. It is possible that there is a systematic error in the nephelometer that affects the backscattering but not the scattering measurements that is not compensated for in the model parameterization. Nephelometer properties that can affect the backscatter relative to total scatter include forward and backward truncation angles, the lambertian characteristics of the light source, and the alignment of the backscatter shutter. Clearly, there is a need to define these properties for each nephelometer used in the field so that the nephelometer response can be modeled accurately.

### 4.3. Light Scattering and Backscattering Apportioned to nss $SO_4^=$ Aerosol

To apportion the total light scattering among aerosol components, the number size distribution was partitioned into an external mixture of nss sulfate aerosol and residual mass. The nss $SO_4^=$ aerosol was assumed to consist of nss $SO_4^=$, $NH_4^+$, and associated $H_2O$ at 30% RH and to contain both the sub- and supermicron fractions. The residual mass was composed of seasalt ions, $NO_3^-$, and $MSA^-$ and was divided into a submicron and supermicron fraction. The apportioned scattering and backscattering coefficients were determined by inserting the size distribution of the sulfate aerosol and residual mass components derived from (8) into (6). Therefore, the apportioned light scattering was derived from the number size distribution using the mass size distributions to estimate the fractions of the sulfate aerosol and the residual mass components within each size bin. The apportioned scattering coefficients are expressed below as fractions of the total measured scattering values.

**Table 3.** Calculated and Measured Values of Scattering and Backscattering Coefficients

| | Scattering Coefficients, $\times 10^{-6}$ m$^{-1}$ | | Backscattering Coefficients, $\times 10^{-6}$ m$^{-1}$ | | |
|---|---|---|---|---|---|
| | $\sigma_{sp,calc}$ | $\sigma_{sp,meas}$ | $\sigma_{bsp,calc}$ | $\sigma_{nbsp,calc}$ | $\sigma_{bsp,meas}$ |
| PSI 91 | 8.1 ± 4.3 | 7.7 ± 3.7 | 0.8 ± 0.38 | 0.84 ± 0.38 | 0.77 ± 0.55 |
| MAGE 92 | 13 ± 0.73 | 13 ± 2.1 | 1.2 ± 0.13 | 1.2 ± 0.12 | 1.9 ± 0.27 |
| Total | 10.3 ± 4.0 | 10.0 ± 3.9 | 0.98 ± 0.35 | 1.01 ± 0.34 | 1.4 ± 0.51 |

Comparison of the average measured light scattering coefficient, $\sigma_{sp,meas}$, and the light scattering coefficient derived from the Mie calculation applied to the number size distribution, $\sigma_{sp,calc}$, for PSI 91 samples ($n$ = 7), MAGE 92 samples ($n$ = 6), and all samples ($n$ = 13). Also compared are the measured backscattering coefficient, $\sigma_{bsp,meas}$, the calculated backscattering coefficient derived from the Mie calculation, $\sigma_{bsp,calc}$, and the calculated backscattering coefficient derived from the nephelometer simulation Mie calculation, $\sigma_{nbsp,calc}$.

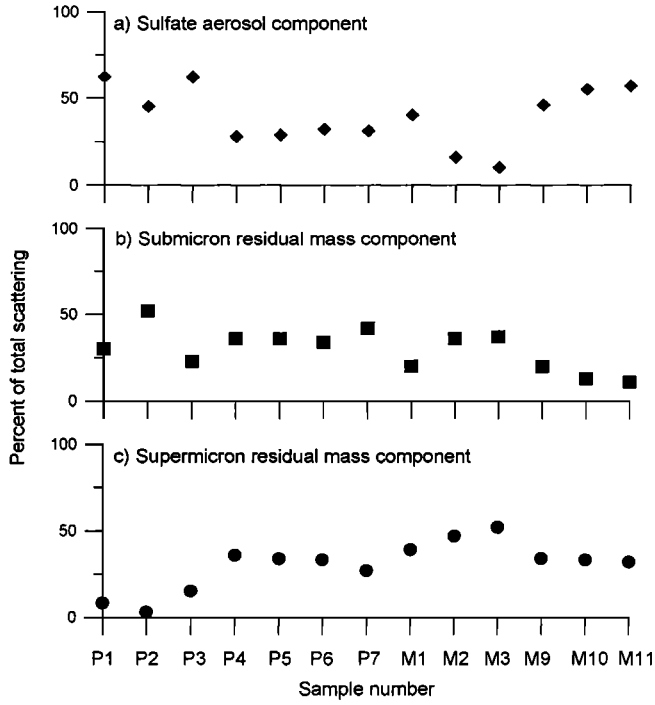


**Figure 14.** Light scattering apportioned to (a) the sulfate aerosol component, (b) the submicron residual mass component, and (c) the supermicron residual mass component expressed as a percent of the calculated total scattering. The apportioned scattering and the total scattering are based on the unmodified Mie calculations. Impactor sample numbers are indicated where P represents PSI 91 and M represents MAGE 92.

For all 13 PSI 91 and MAGE 92 samples, the portion of the total measured $\sigma_{sp,meas}$ due to nss $SO_4^=$ aerosol ranged from 10.5 to 62% and with an average and standard deviation of 39 ± 16% (Figure 14). The fraction of $\sigma_{bsp,meas}$ apportioned to nss $SO_4^=$ aerosol ranged from 6 to 61% with an average and standard deviation of 37 ± 18%. Low sulfate-apportioned scattering values are expected if the sulfate mass fraction, or amount of nss $SO_4^=$ and $NH_4^+$ relative to the total mass, is small. The lowest calculated percent values for the contribution of nss $SO_4^=$ aerosol to light scattering occurred for samples M2 (6%), M3 (11%), and P4 (28%). Correspondingly, these three samples had the lowest mass fractions of nss $SO_4^=$ and $NH_4^+$. A comparison of large apportioned scattering percent values for nss $SO_4^=$ aerosol with the mass fraction of sulfate and ammonium does not reveal a simple relationship, however. Samples P1 and P3 had the highest sulfate-apportioned scattering percent values (both at 62%) but a relatively low mass fraction of nss $SO_4^=$ and $NH_4^+$. The P1 and P3 size distributions of nss $SO_4^=$ and $NH_4^+$ indicate that the majority of the mass occurred between 0.3 and 0.7 μm, within the most efficient size range for scattering. Alternatively, sample P2 had the highest mass fraction of nss $SO_4^=$ and $NH_4^+$ but only a moderate sulfate-apportioned scattering percent value (45%). For this case, the nss $SO_4^=$ and $NH_4^+$ size distributions indicate that much of the mass occurred outside of the most efficient size range for light scattering.

### 4.4. Calculation of the Sulfate Scattering to Mass Ratio

Scattering to mass ratios traditionally have been obtained by a linear regression of the measured mass concentration of each aerosol component against the total measured scattering coefficient [*White and Roberts*, 1977; *White*, 1986; *Hegg et al.*, 1993]. A similar approach was followed here to calculate the scattering to mass ratio of the sulfate ion ($\alpha_{sp,SO4,ion}$) including both the sub- and supermicron fractions, the submicron residual mass ($\alpha_{sp,res1}$), and the supermicron residual mass ($\alpha_{sp,res2}$). The calculation was based on the measured scattering coefficients, the measured mass concentration of nss $SO_4^=$ summed over all impactor stages, and the residual mass concentrations estimated from (7) and the density of seasalt. A regression of the following form was used

$$\sigma_{sp(meas)} = \alpha_{sp,SO4,ion} m_{SO4,ion} + \alpha_{sp,res1} m_{res1} + \alpha_{sp,res2} m_{res2} \quad (14)$$

to yield a scattering to mass ratio of the form shown in (13). A similar regression was calculated for the backscattering to mass ratios. The regression calculations assume that only the measured chemical species contribute to $\sigma_{sp(meas)}$. Hence the resulting scattering to mass ratios may overestimate the scattering due to nss $SO_4^=$ aerosol and seasalt.

Scattering to mass ratios based on Mie theory were estimated from the scattering and backscattering values apportioned to the total sulfate component (sub- and supermicron fractions), the submicron residual component, and the supermicron residual component. The estimates of the scattering to mass ratios and backscattering to mass ratios from the linear regression and Mie calculations are compared in Table 4. For all three aerosol components, the results from the linear regression and the Mie calculations agreed well. The average and standard deviation of $\alpha_{sp,SO4,ion}$ was 5.0 ± 1.6 $m^2\ g^{-1}$ from the Mie calculation, while the regression-derived value was 3.6 ± 1.1 $m^2\ g^{-1}$. Values of $\alpha_{bsp,SO4,ion}$ were 0.41 ± 0.04 $m^2\ g^{-1}$ from the Mie calculation and 0.38 ± 0.11 $m^2\ g^{-1}$ from the linear regression.

**Table 4.** Mean and Standard Deviation of the Scattering to Mass and Backscattering to Mass Ratios Derived from the Mie Calculation and the Linear Regression for all 13 PSI 91 and MAGE 92 Samples

| Ratio, $m^2\ g^{-1}$ | Mie Calculation | Regression |
|---|---|---|
| | *Scattering* | |
| $\alpha_{sp,SO4,ion}$ | 5.0 ± 1.6 | 3.6 ± 1.1 ($r^2$ = 0.63) |
| $\alpha_{sp,SO4,aer}$ | 2.8 ± 0.85 | |
| $\alpha_{sp,res1}$ | 3.6 ± 0.47 | 4.3 ± 1.3 |
| $\alpha_{sp,res2}$ | 0.87 ± 0.057 | 0.6 ± 0.18 |
| | *Backscattering* | |
| $\alpha_{bsp,SO4,ion}$ | 0.41 ± 0.04 | 0.38 ± 0.11 ($r^2$ = 0.78) |
| $\alpha_{bsp,SO4,aer}$ | 0.23 ± 0.027 | |
| $\alpha_{bsp,res1}$ | 0.33 ± .011 | 0.34 ± 0.102 |
| $\alpha_{bsp,res2}$ | 0.094 ± 0.012 | 0.14 ± 0.042 |

The value $\alpha_{sp,SO4,ion}$ refers to the sulfate-apportioned light scattering per unit mass of submicron plus supermicron sulfate ion; $\alpha_{sp,SO4,aer}$ refers to the sulfate-apportioned light scattering per unit mass of submicron plus supermicron sulfate aerosol; $\alpha_{sp,res1}$ refers to the light scattering apportioned to the submicron residual mass per unit mass of the submicron residual component; and $\alpha_{sp,res2}$ refers to the light scattering apportioned to the supermicron residual mass per unit mass of the supermicron residual component.

The variability in $\alpha_{sp,SO4,ion}$ is a result of variability in the size distribution of the sulfate aerosol component. In the cases with the largest scattering to mass ratios (M2 and M3), the sulfate was found exclusively in the 0.5 to 1.0 μm size range. As this is an efficient size range for light scattering, these high values of $\alpha_{sp,SO4,ion}$ were not "diluted" by coarse mode sulfate as was the case for the other samples. Omitting samples M2 and M3 yielded a lower average $\alpha_{sp,SO4,ion}$ value of 4.4 ± 0.62 $m^2$ $g^{-1}$. The backscattering to mass ratios were insensitive to the variable size distribution of the sulfate component. Omitting M2 and M3 from $\alpha_{bsp,SO4,ion}$ yielded a negligibly lower value of 0.39 ± 0.03 $m^2$ $g^{-1}$.

Ratios of scattering to the mass of sulfate aerosol, $\alpha_{sp,SO4,aer}$, as defined by (11), also were estimated from the Mie apportionment calculations and found to have an average and standard deviation of 2.8 ± 0.85 $m^2$ $g^{-1}$. These values are lower than those for the sulfate ion as the additional mass of associated $NH_4^+$ and $H_2O$ is included. The average backscattering to mass ratio of the sulfate aerosol, $\alpha_{bsp,SO4,aer}$, was 0.23 ± 0.027 $m^2$ $g^{-1}$.

The scattering to mass and backscattering to mass ratios of the submicron residual component were only slightly lower than values for the sulfate ion indicating that the submicron residual mass was composed of species with similar scattering properties as sulfate aerosol. Values for the supermicron residual component were considerably lower than those for the submicron residual component, presumably due to the inefficient scattering associated with this particle size range.

## 5. Comparison of Parameters Derived from PSI 91 and MAGE 92 and Those Used in Global Climate Models

A comparison of model- and empirically derived parameters needed in the calculation of the direct effect is shown in Table 5. These parameters were obtained from the global climate models of *Charlson et al.* [1991] and *Kiehl and Briegleb* [1993] and from measurements made during PSI 91 and MAGE 92. *Kiehl and Briegleb* [1993] assumed a $D_{gn}$ of 0.1 μm and a $\sigma_{sg}$ of 2.0 based on measurements of anthropogenic aerosol. Values of $D_{gn}$ during PSI 91 and MAGE 92 for diameters between 0.1 and 0.8 μm averaged 0.19 ± 0.02 and 0.19 ± 0.035 μm, respectively. The higher values of $D_{gn}$ for PSI 91 and MAGE 92 relative to those of the anthropogenic aerosol assumed by *Kiehl and Briegleb* [1993] are unexpected as they are based on air masses of a presumably more marine nature. Average values of $\sigma_{sg}$ during PSI 91 and MAGE 92 for this same size range were 1.4 ± 0.053 and 1.4 ± 0.06. The smaller values of $\sigma_{sg}$ for PSI 91 and MAGE 92 correspond to a more marine aerosol.

The optical properties that were compared include the backscattered fraction, $b$, the asymmetry parameter, $g$, and the scattering to mass ratio for the sulfate ion. The value of the backscattered fraction applied in climate models has a significant influence on the magnitude of the calculated reflected flux. The asymmetry parameter, $g$, is an intensity-weighted average of the cosine of the scattering angle and is a measure of the degree of backscattering used in radiative transfer models. *Kiehl and Briegleb* [1993] used a value of $g$ equal to 0.69 at visible wavelengths, which can be converted to a backscattered fraction of 0.1 by assuming a Henyey-Greenstein phase function [*Wiscombe and Grams*, 1976]. This value of $g$ was based on the assumption of a lognormal size distribution, an aerosol chemical composition of 75% $H_2SO_4$ and 25% $H_2O$, and Mie theory. *Charlson et al.* [1991] used a backscattered fraction of 0.15, which corresponds to $g$ = 0.52, based on measurements of anthropogenic aerosol. The average and standard deviation of the measured values of $b$ from PSI 91 and MAGE 92 were 0.15 ± 0.009 and 0.15 ± 0.009, respectively. Values of $g$ based on the Mie calculations were 0.66 ± 0.036 (PSI 91) and 0.69 ± 0.008 (MAGE 92). The average and standard deviation of calculated values of $b$ were 0.1 ± 0.006 (PSI 91) and 0.092 ± 0.006 (MAGE 92).

It is not surprising that values of $b$ used by *Charlson et al.* [1991] and those measured during PSI 91 and MAGE 92 agree, as they are based on observations using the same instrumental technique. The standard deviations of the measured values of $b$ are small indicating that $D_{gn}$, $\sigma_{sg}$, and the aerosol refractive index remained constant during both field experiments. The backscattered fraction calculated by *Kiehl and Briegleb* [1993] and for PSI 91 and MAGE 92 were lower than the measured values. This difference could be a result of measurement characteristics of the nephelometer that affect backscattering and not scattering. Further observations which allow for a compari-

**Table 5.** Comparison of Parameters Derived from PSI 91 and MAGE 92 to Those Used in Two Global Climate Models

| Parameter | Model | | PSI 91 | MAGE 92 |
|---|---|---|---|---|
| | *Charlson et al.* [1991] | *Kiehl and Briegleb* [1993] | | |
| $D_{gn}$, μm for $0.1 < D_p < 0.8$ | NA | 0.1 | 0.19 ± 0.02 | 0.19 ± 0.035 |
| $\sigma_{sg}$ for $0.1 < D_p < 0.8$ | NA | 2.0 | 1.4 ± 0.053 | 1.4 ± 0.06 |
| asymmetry parameter, $g$ | NA | 0.69 (visible) | 0.66 ± 0.036 | 0.69 ± 0.008 |
| backscattered fraction, $b$ | 0.15 | 0.1 (visible) | Measured: 0.15 ± 0.009 | 0.15 ± 0.009 |
| | | | Calculated: 0.1 ± 0.006 | 0.092 ± 0.006 |
| $\alpha_{sp,SO4,ion}$, $m^2$ $g^{-1}$ | 5 | 5 (550 nm) | Calculated: 4.1 ± 0.48 | 6.01 ± 1.8 |

NA, not available.

son between total measured and calculated light scattering and backscattering are needed under a variety of atmospheric conditions.

The scattering to mass ratio also has a large effect on the calculated magnitude of sulfate aerosol forcing. In comparing values of $\alpha_{sp,SO4,ion}$ derived from different sources, it is necessary to be aware of the many definitions that are used for this term. The values used in the *Charlson et al.* [1991] and *Kiehl and Briegleb* [1993] models include only $SO_4^=$ mass in the submicron fraction of the aerosol. Those derived from PSI 91 and MAGE 92 take into account the nss $SO_4^=$ mass for all particles less than 10 μm in diameter. In addition, *Charlson et al.* [1991] use the total measured light scattering coefficient in their calculation while *Kiehl and Briegleb* [1993] and values from PSI 91 and MAGE 92 consider only light scattering due to sulfate aerosol.

*Charlson et al.* [1991] used a uniform value of $\alpha_{sp,SO4,ion}$ of 5 $m^2 g^{-1}$ and applied it globally. This value is based on empirical measurements of sulfate haze over northern Europe. *Kiehl and Briegleb* [1993] allowed $\alpha_{sp,SO4,ion}$ to vary with wavelength and employed a value of 5 $m^2 g^{-1}$ at 550 nm. As the incident wavelength increases, however, $\alpha_{sp,SO4,ion}$ decreases, resulting in a smaller aerosol forcing. Average sulfate scattering to mass ratios for PSI 91 and MAGE 92 were 4.1 ± 0.48 and 6.01 ± 1.8 $m^2 g^{-1}$, respectively. The relative deviation of approximately ±33% for these scattering to mass ratios are the standard deviations over the 13 PSI 91 and MAGE 92 samples divided by the mean values. Although there was considerable variability in $\alpha_{sp,SO4,ion}$ over the regions studied, it was less than the 40% relative uncertainty estimated by *Charlson et al.* [1992]. Further measurements are needed to assess the variability in $\alpha_{sp,SO4,ion}$ on a global basis for aerosol derived from anthropogenic, marine, and continental sources.

## 6. Conclusions

Calculation of the magnitude of the direct effect of sulfate aerosol on climate is sensitive to the optical, physical, and chemical properties of the aerosol that serve as model input. Discrepancies exist between measured and calculated values of aerosol properties which can lead to large differences in these model calculations. In addition, aerosol optical, physical, and chemical properties vary temporally and spatially, making their inclusion in climate models even more complex. The data set presented here has provided an opportunity to compare measured and calculated values of light scattering and backscattering and to assess the regional and temporal variability of these parameters.

Measurements made during PSI 91 and MAGE 92 indicate that there is a great deal of spatial and temporal variability in the concentrations of nss $SO_4^=$, $NH_4^+$, and $Na^+$ as a function of particle size. In addition, the mass analyzed by ion chromatography during PSI 91 only accounted for 42 to 62% of the total aerosol mass indicating that an unidentified mass component also has a variable concentration. The optical properties of the aerosol also were variable with measured values of $\sigma_{sp,meas}$ ranging between 3.7 and 15 × $10^{-6}$ $m^{-1}$ and $\sigma_{bsp,meas}$ ranging between 0.63 and 2.2 × $10^{-6}$ $m^{-1}$. The backscattered fraction showed little variability, however, indicating that the shape of the number size distribution and the aerosol refractive index remained fairly constant.

A Mie model was applied to the measured number size distributions to calculate light scattering and backscattering coefficients. The mean calculated scattering coefficient was 3% higher than the mean measured value and the variance around this mean was within the uncertainty of the calculations. Hence, the scattering characteristics of the aerosol were well represented by the model and closure was achieved for the scattering coefficient. The calculated backscattering coefficient was about 40% lower than the measured values. An attempt to improve this agreement by including a parameterization of nephelometer properties within the model was unsuccessful. It is possible that there was a systematic error in the nephelometer measurements that affected the backscattering but not scattering measurements. This error was not compensated for by using the *Heintzenberg* [1978] angular sensitivity functions.

Measured values of the backscattered fraction agreed well with the nephelometer-derived value used in the *Charlson et al.* [1991] model. Calculated values of $b$ from PSI 91, MAGE 92, and the *Kiehl and Briegleb* [1993] model, however, were lower than these measured values. Further observations are needed that will allow for a direct comparison of measured and calculated aerosol optical properties for a variety of aerosol types and atmospheric conditions. In addition, the measurement properties of each nephelometer used in the field should be determined so that they can be accurately parameterized within the Mie model calculations of the backscattering coefficient.

Based on Mie apportionment calculations, 10.6 to 62% of the total measured light scattering was due to nss $SO_4^=$ aerosol. The lowest sulfate-apportioned scattering values corresponded to samples containing the lowest mass fractions of sulfate aerosol. Samples with high mass fractions of sulfate aerosol or with the majority of the sulfate occurring in the 0.3 to 0.7 μm size range had the highest sulfate-apportioned scattering values.

The average and standard deviation of the sulfate ion scattering to mass ratio, $\alpha_{sp,SO4,ion}$, calculated from Mie theory applied to the measured number and mass size distributions during PSI 91 and MAGE 92 was 5.0 ± 1.6 $m^2 g^{-1}$ for the dry aerosol at 30% RH. Variability in $\alpha_{sp,SO4,ion}$ was due to variability in the number size distribution of the aerosol. This average value agreed well with the values used by the climate models of *Charlson et al.* [1991] and *Kiehl and Briegleb* [1993].

The measurements described here represent an initial attempt to characterize $\alpha_{sp,SO4,ion}$ for marine aerosol. As $\alpha_{sp,SO4,ion}$ is dependent on aerosol chemical composition, further measurements are needed to determine its magnitude for marine, continental, and anthropogenic aerosol. These measurements should include the determination of scattering and backscattering coefficients at more than one wavelength to test the validity of the use of wavelength-independent parameters in climate models. The ultimate goal of such a measurement program is the development of a global-scale database to reveal the extent of the spatial, temporal, and spectral variability in the aerosol properties relevant to climate forcing.

**Acknowledgments.** We thank L. McInnes and C. Zenker for analytical assistance, T. Anderson, W. Asher, and R. Charlson for helpful discussions, and the officers and crew of the *Vickers* and *Discoverer* for their cooperation. This research was funded by the Marine Sulfur, Aerosol, and Climate Component of the NOAA Climate and Global Change Program and is a contribution to the International Global Atmospheric Chemistry (IGAC) Core Project of the International Geosphere-Biosphere Programme (IGBP). This is NOAA PMEL contribution 1561. S. F. Marshall acknowledges support from the National Science Foundation (ATM-9320871) and from the Department of Energy's National Institute for Global Environmental Change through its Western Regional Center.

## References


Baron, P. A., Calibration and use of the aerodynamic particle sizer (APS 3300), *Aerosol Sci. Technol., 5*, 55–67, 1986.

Berner, A., C. Lurzer, F. Pohl, O. Preining, and P. Wagner, The size distribution of the urban aerosol in Vienna, *Sci. Total Environ., 13*, 245–261, 1979.

Bray, W. H., Water vapor pressure control with aqueous solutions of sulfuric acid, *J. Mater., 5*, 233–248, 1970.

Charlson, R. J., R. F. Pueschel, and H. Horvath, The direct measurement of atmospheric light scattering coefficient for studies of visibility and air pollution, *Atmos. Environ., 1*, 469–478, 1967.

Charlson, R. J., D. S. Covert, and T. V. Larson, Observation of the effect of humidity on light scattering by aerosols, in *Hygroscopic Aerosols*, edited by L. H. Ruhnke and A. Deepak, pp. 35–44, A. Deepak Publishing, Hampton, Va., 1984.

Charlson, R. J., J. Langner, H. Rodhe, C. B. Leovy, and S. G. Warren, Perturbation of the northern hemisphere radiative balance by backscattering from anthropogenic sulfate aerosols, *Tellus, 43B*, 152–163, 1991.

Charlson, R. J., S. E. Schwartz, J. M. Hales, R. D. Cess, J. A. Coakley, Jr., J. E. Hansen, and D. J. Hofmann, Climate forcing by anthropogenic aerosols, *Science, 255*, 423–430, 1992.

Draxler, R. R., Hybrid Single-Particle Lagrangian Integrated Trajectories (HY-SPLIT): Version 3.0. User's Guide and Model Description, *Tech. Rep. ERL ARL-195*, NOAA, Silver Spring, Md., 1992.

Hegg, D. A., R. J. Ferek, and P. V. Hobbs, Light scattering and cloud condensation nucleus activity of sulfate aerosol measured over the northeast Atlantic Ocean, *J. Geophys. Res., 98*, 14,887–14,894, 1993.

Heintzenberg, J., The angular calibration of the total scatter/backscatter nephelometer, consequences and applications, *Staub Reinhalt. Luft, 38*, 62–63, 1978.

Holland, H. D., *The Chemistry of the Atmosphere and Oceans*, p. 154, John Wiley, New York, 1978.

Keady, P. B., F. R. Quant, and G. S. Sem, Differential mobility particle sizer: a new instrument for high resolution aerosol size distribution measurements below 1 μm, *TSI Q., 9*, 3–11, 1983.

Kent, G. S., et al., Modeling atmospheric aerosol backscatter at $CO_2$ laser wavelengths, 1, Aerosol properties, modeling techniques, and associated problems, *Appl. Opt., 22*, 1655–1665, 1983.

Kiehl, J. T., and B. P. Briegleb, The relative roles of sulfate aerosols and greenhouse gases in climate forcing, *Science, 260*, 311–314, 1993.

Liu, B. Y. H., and K. W. Lee, Efficiency of membrane and Nuclepore filters for sub-micrometer aerosols, *Environ. Sci. Technol., 10*, 345–350, 1976.

Liu, B. Y. H., and D. Pui, On the performance of the electrical aerosol analyzer, *J. Aerosol Sci., 6*, 249–264, 1975.

London, J., A study of the atmospheric heat balance, *Rep. AFCRC-TR-57-287*, Air Force Geophysics Lab., Hanscom Field, Mass., 1957.

Marshall, S. F., Measurement-derived radiative transfer parameters for the aerosol climate forcing problem, M.S. dissertation, University of Washington, Seattle, Wash., 1994.

Palmer, K. F., and D. Williams, Optical constants of sulfuric acid; application to the clouds of Venus? *Appl. Opt., 14*, 208–219, 1975.

Penner, J. E., R. J. Charlson, J. M. Hales, N. S. Laulainen, R. Leifer, T. Novakov, J. Ogren, L. F. Radke, S. E. Schwartz, and L. Travis, Quantifying and minimizing uncertainty of climate forcing by anthropogenic aerosols, *Bull. Am. Meteorol. Soc., 75*, 375–400, 1994.

Quinn, P. K., D. S. Covert, T. S. Bates, V. N. Kapustin, D. C. Ramsey-Bell, and L. M. McInnes, Dimethylsulfide/cloud condensation nuclei/climate system: Relevant size-resolved measurements of the chemical and physical properties of atmospheric aerosol particles, *J. Geophys. Res., 98*, 10,411–10,427, 1993.

Reineking, A., and J. Porstendorfer, Measurements of particle loss functions in a differential mobility analyzer for different flow rates, *Aerosol Sci. Technol., 5*, 483–487, 1986.

Sloane, C. S., Optical properties of aerosols of mixed composition, *Atmos. Environ., 4*, 871–878, 1984.

Stelson, A. W., Urban aerosol refractive index prediction by partial molar refraction approach, *Environ. Sci. Technol., 24*, 1676–1679, 1990.

Tang, I. N., and H. R. Munkelwitz, Simultaneous determination of refractive index and density of an evaporating aqueous solution droplet, *Aerosol. Sci. Technol., 15*, 201–207, 1991.

Tang, I. N., and H. R. Munkelwitz, Water activities, densities, and refractive indices of aqueous sulfate and nitrate droplets of atmospheric importance, *J. Geophys. Res., 99*, 18,801–18,808, 1994.

Twomey, S., *Atmospheric Aerosols*, Elsevier, New York, 1977.

Vanderpol, A. H., A systematic approach for computer analysis of air chemistry data, Ph.D. dissertation, University of Washington, Seattle, Wash., 1975.

Waggoner, A. P., A. J. Vanderpol, R. J. Charlson, S. Larsen, L. Granat, and C. Tradgard, Sulfate light scattering ratio as an index of the role of sulfur in the tropospheric optics, *Nature, 261*, 120–122, 1976.

Wang, H., and W. John, Characteristics of the Berner impactor for sampling inorganic ions, *Aerosol. Sci. Technol., 8*, 157–172, 1988.

Weiss, R. E., T. V. Larson, and A. P. Waggoner, In situ rapid-response measurements of $H_2SO_4/(NH_4)_2SO_4$ aerosols in rural Virginia, *Environ. Sci. Technol., 16*, 525–532, 1982.

Whitby, K. T., The physical characteristics of sulfur aerosols, *Atmos. Environ., 12*, 135–159, 1978.

White, W. H., On the theoretical and empirical basis for apportioning extinction by aerosols: A critical review, *Atmos. Environ., 20*, 1659–1672, 1986.

White, W. H., and P. T. Roberts, On the nature and origins of visibility-reducing aerosols in the Los Angeles air basin, *Atmos. Environ., 11*, 803–812, 1977.

Wiscombe, W. J., and G. W. Grams, The backscattered fraction in two-stream approximations, *J. Atmos. Sci., 33*, 2440–2451, 1976.

Zang, Z., and B. Y. H. Liu, Performance of TSI 3760 condensation nuclei counter at reduced pressures and flow rates, *Aerosol Sci. Technol., 15*, 228–238, 1991.



T. S. Bates, V. N. Kapustin, and P. K. Quinn, NOAA/PMEL, 7600 Sand Point Way, N.E., Seattle, WA 98115. bates@pmel.noaa.gov; kapustin@pmel.noaa.gov; quinn@pmel.noaa.gov.

D. S. Covert and S. F. Marshall, Department of Atmospheric Sciences, University of Washington, Seattle, WA 98195. dcovert@u.washington.edu; stephen@atmos.washington.edu.


(Received June 20, 1994; revised December 19, 1994; accepted January 20, 1995.)